Electronic Supplementary Material (ESI) for Physical Chemistry Chemical Physics.

Exploring exchange processes in proteins by paramagnetic perturbation of NMR spectra

Yamanappa Hunashal[a,b], Cristina Cantarutti[c], Sofia Giorgetti[d], Loredana Marchese[d], Henriette Molinari[e], Neri Niccolai[f], Federico Fogolari[g,h], Gennaro Esposito[a,h*]

[a] Science Division, New York University Abu Dhabi, Abu Dhabi – UAE.
[b]DAME, Università di Udine, 33100 Udine, Italy.
[c]Institute of Chemistry, UMR CNRS 7272, Université Côte d'Azur, University of Nice Sophia Antipolis, Parc Valrose, 06108, Nice Cedex 2, France.
[d]Dipartimento di Medicina Molecolare, Università di Pavia, Via Taramelli 3, 27100 Pavia, Italy.
[e]Istituto di Scienze e Tecnologie Chimiche (SCITEC), CNR, Via A. Corti, 12, 20133, Milano, Italy. [f]Dipartimento di Biotecnologie, Chimica e Farmacia, Università di Siena, Via Moro 2, 53100 Siena, Italy. [g]DMIF, Università di Udine, 33100 Udine, Italy.
[h]INBB, Viale Medaglie d'Oro 305, 00136 Roma, Italy.

*Corresponding author
rino.esposito@nyu.edu (Gennaro Esposito)

ELECTRONIC SUPPLEMENTARY INFORMATION

Figure S1: Overlay of the A_N values obtained from ^{1}H-^{15}N HSQC spectra of 0.32 mM β2m in the presence of 1.6 mM Tempol at 298 K, with relaxation delay of 0.2 s (green), 0.5 s (blue) and 4 s (red). The β-strand location and naming along the sequence is reported with yellow strips. The β-strand location and naming along the sequence is reported with yellow strips.

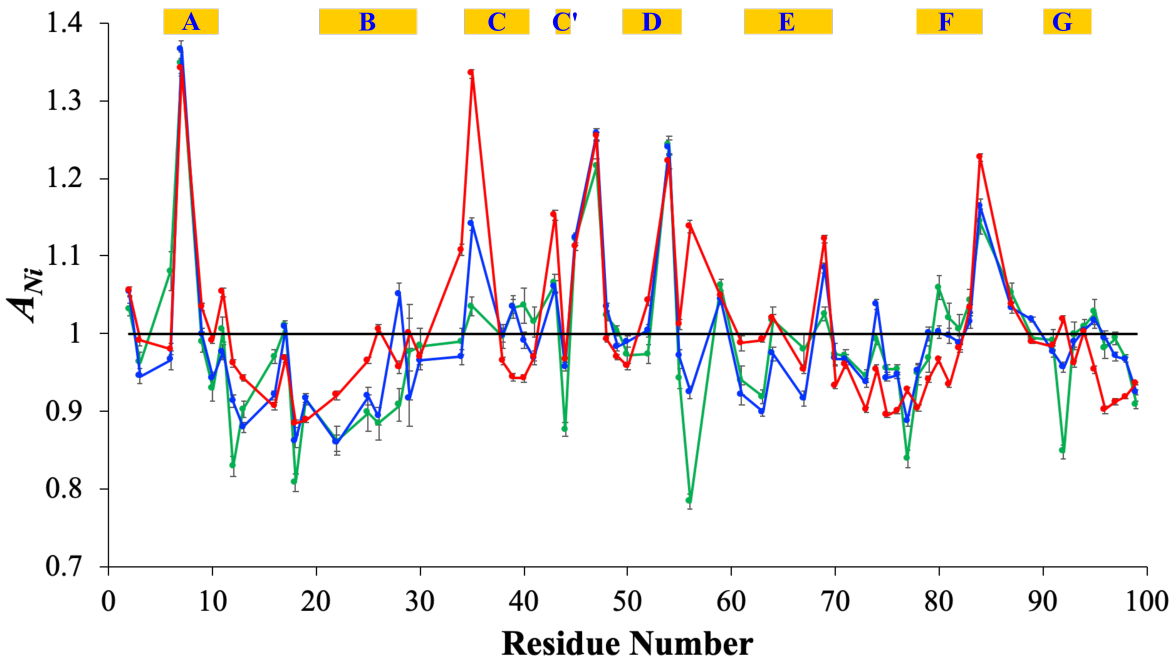

Figure S2: (A) Amide hydrogen chemical shifts of a selected group of β2m residues measured as a function of the Tempol/ protein concentration ratio (R). (B) Overlay of ESR spectra of Tempol (blue) and Tempol: β2m, 1:1 (red) and Tempol: β2m, 1:5 (green).

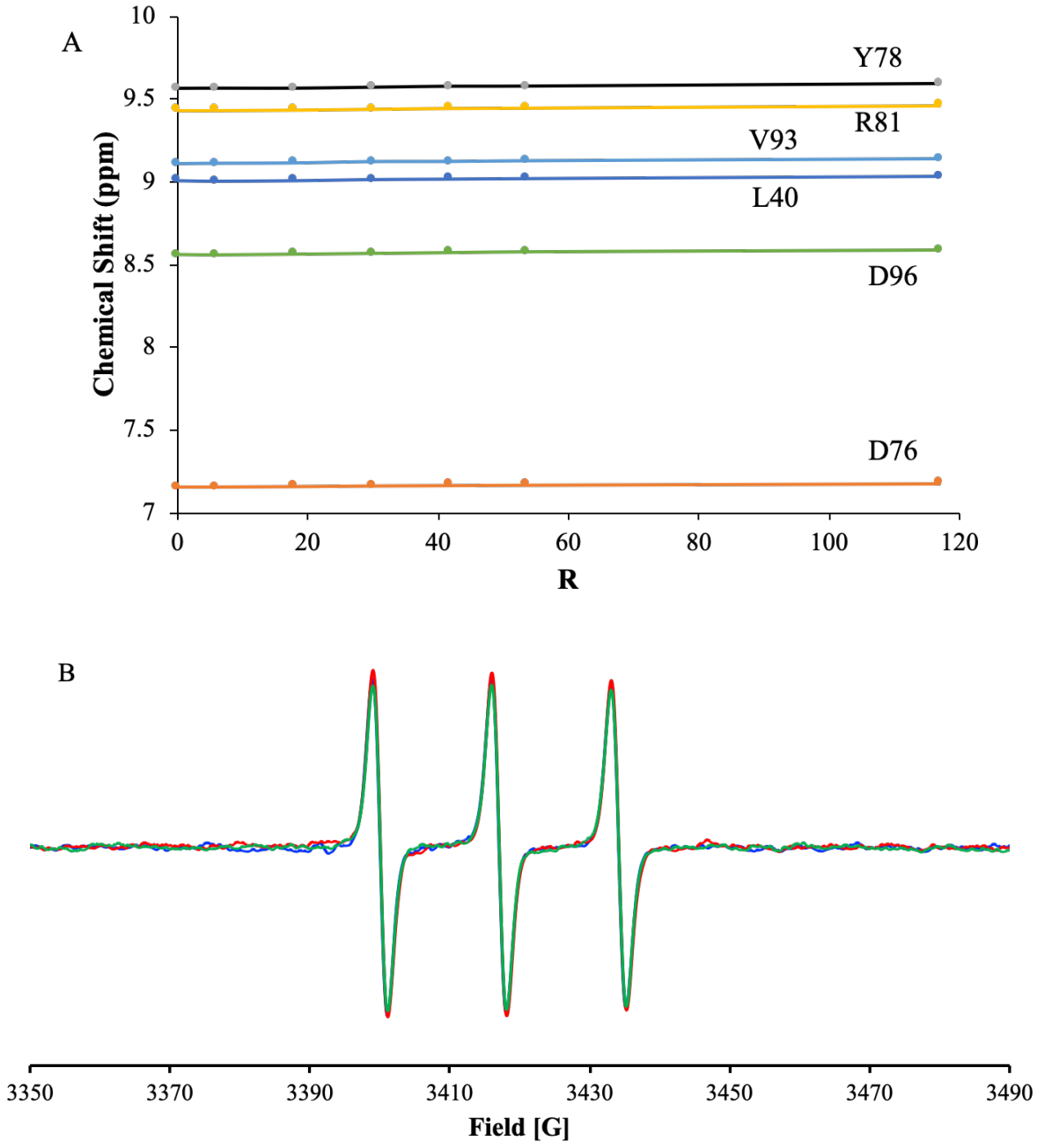

Figure S3: Relative intensity of individual backbone NH signals from HSQC spectra measured for 0.32 mM β2m samples, with and without 1.6 mM Tempol, at different temperatures and relaxation delays (D1): (A) D1= 0.5 s at 298 K; (B) D1= 4 s at 298 K; (C) D1=0.5 s at 310 K; (D) D1=5 s at 310 K. The red and green lines represent the average relative intensity and the displacement by one standard deviation, respectively.

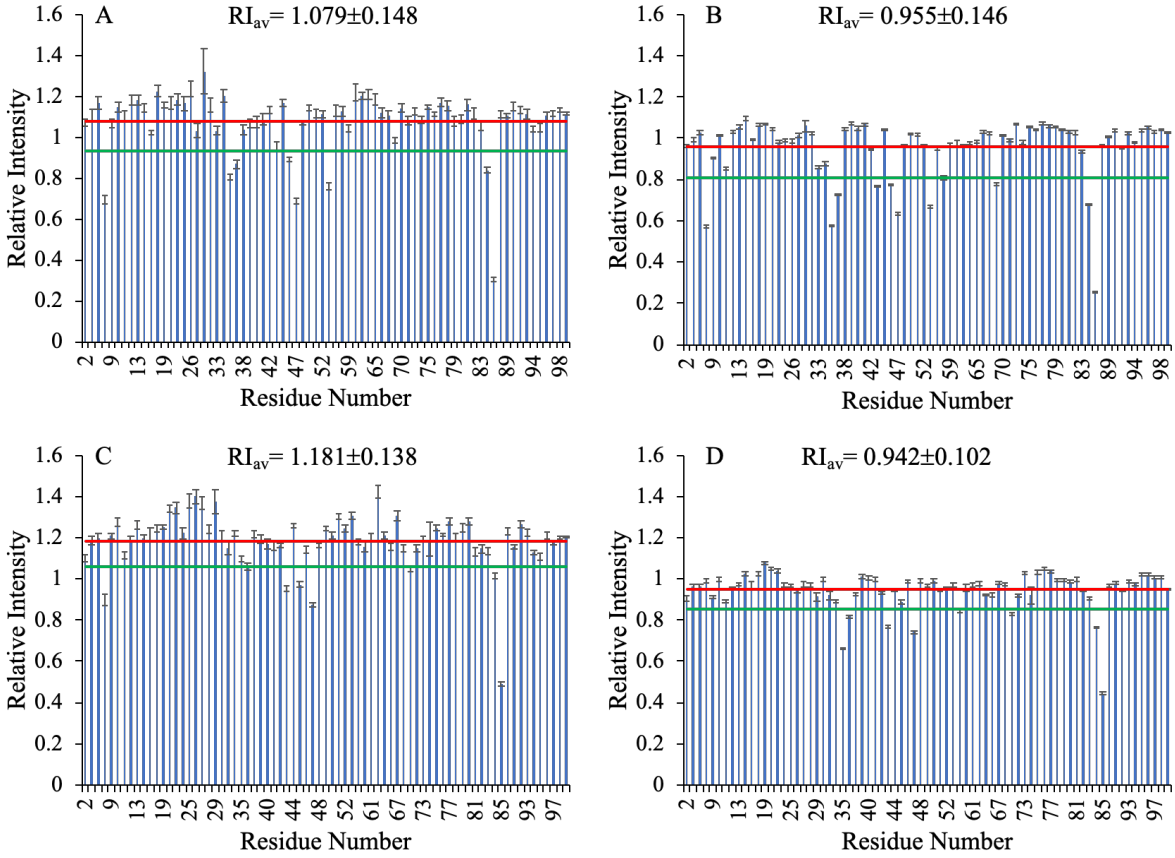

Figure S4: Relative intensity of individual backbone NH signals from HSQC spectra measured for 50 μM β2m samples, with and without 250 μM Tempol, at 298 K and different relaxation delays (D1): (A) D1= 0.5 s; (B) D1= 4 s. The red and green lines represent the average relative intensity and the displacement by one standard deviation, respectively.

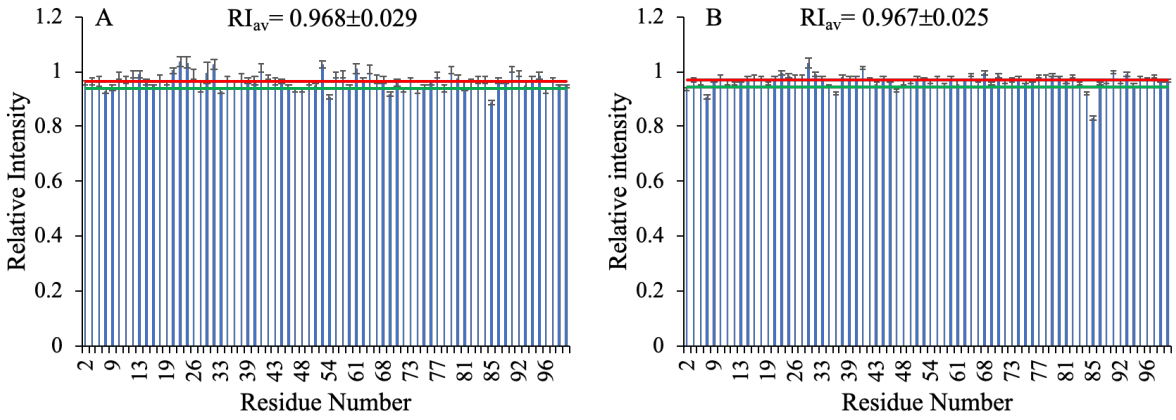

Figure S5: (A) Average depth from surface of β_2m amide hydrogens throughout 100 ns MD simulation[a]. (B) Experimental A_N [*eq*] values against computed average depth of β2m amide hydrogens. The correlation has a *p* value of 4.5×10^{-4} and is therefore statistically meaningful.

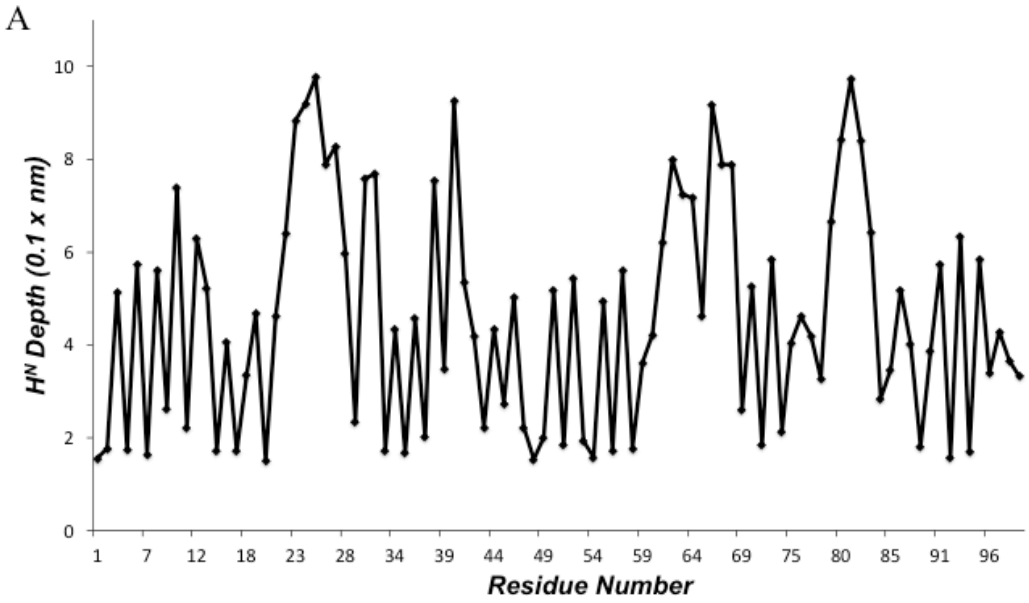

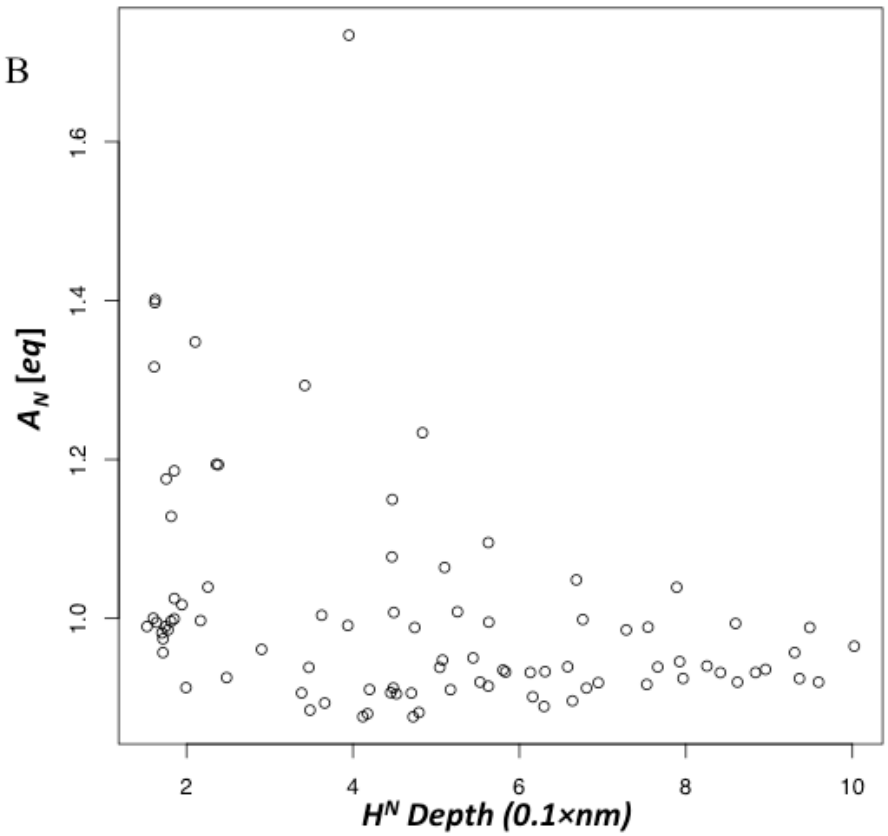

[a]The coordinates of β2m were obtained from the structure of human class I major histocompatibility complex (PDB code: 3HLA)[1]. The protonation states of titratable groups were assigned using the Bluues server available at the URL http://protein.bio.unipd.it/bluues/ [2,3]. For TEMPOL the structure was built using, as a starting template, the structure of the spin label reported by Sezer et al.[4], then adapting the parameters from CHARMM forcefield with the charges assigned using the algorithm of Gasteiger and Marsili[5]. Molecular dynamics simulations were carried out with the program NAMD 2.9[6] using the Generalized Born Surface Area (GBSA) implicit solvent model[7] employing the Onufriev-Bashford-Case (OBC) model[8]. A high concentration box with 26 TEMPOL molecules arranged on a cubic grid surrounding a protein molecule was simulated imposing elastic spherical boundary conditions[9]. Four 5 ns simulations were conducted at 298 K and 310 K. Reference explicit solvent simulations were performed for 110 ns at 298 K and 310 K essentially as previously described[10]. Analysis was performed on the last 100 ns. The depth of amide protons was obtained as the generalized Born radius computed according to the GBR6 model[1,11]. The molecular surface was generated using the program MSMS[12] and the GBR6 was computed using the program Bluues[1]. For all the exposed locations listed in Table 1of main text, the corresponding amide hydrogens possess average distances from the surface between 0.18 and 0.49 nm. A qualitative correlation also emerges between the extent of attenuation and the depth figure, i.e. the larger the depth, the lower the attenuation.

Figure S6: (A) NMR experiment carried out on HOD, in the absence and presence of Tempol, to highlight the enhanced recovery of the off-equilibrium magnetization[a]. Below the ^{1}H pulse line, the G line indicates the magnetic gradient pulse timing. (B) HOD signal intensity as a function of the B (magnetic field induction) gradient strength obtained with the sequence sketched in panel A, in the absence (black) and in the presence of 10 mM (blue) or 100 mM (red) Tempol. Each series of values was normalized to the respective value obtained at zero B gradient. (C) Same as in panel B, but with double normalization for the data acquired in presence of Tempol, namely with an additional initial scaling with respect to the corresponding intensities sampled in the absence of Tempol, prior to applying the zero-gradient-value normalization within each series.

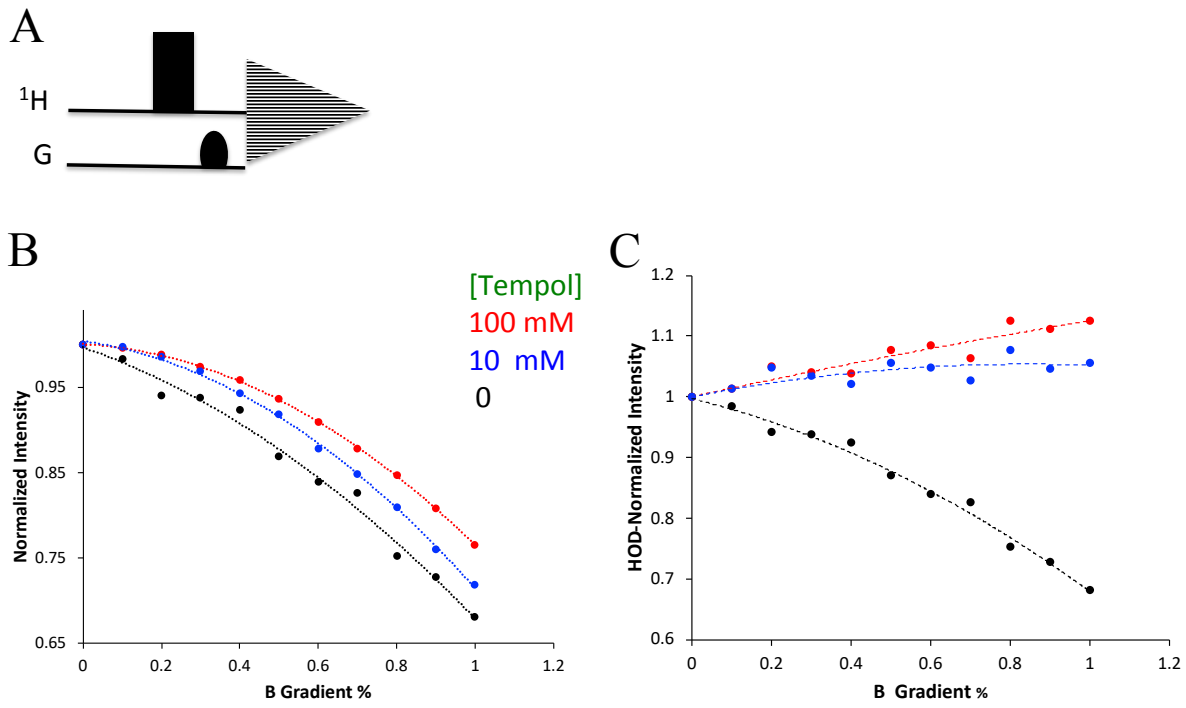

[a]The experiments were acquired at 600 MHz and 298 K with 1% H_2O in D_2O samples at varying Tempol concentrations (0, 10, 100 mM), by collecting 16 scans preceded by 64 dummy scans with a relaxation delay (D1) of 0.2 s. A magnetic field gradient along the *z*-direction was applied with a 100 μs pulse of differing strengths, i.e. 0-1% with respect to the maximum of 67 Gauss/cm. To demonstrate the Tempol-induced enhancement of the signal acquired with short relaxation delay, the sequence included a small field gradient between the pulse and the acquisition. The gradient should represent the dephasing contributed by slow or intermediate exchange processes. Expectedly, if the experiment is done comparing pure HOD and Tempol-doped HOD as a function of the gradient strength, a larger recovery should be obtained from doped HOD because of the effect of $R_{1\rho}$. The effect should increase on increasing the gradient. The results confirm the expectations.

Figure S7: Fitting (blue curve) of 0.36 mM β2m relaxation dispersion data. The plots report the transverse relaxation rate (s^{-1}) as a function of the 180° pulse spacing (s^{-1}). (A) 298 K; (B) 310 K. The experimental data points (red circles) are reported with the corresponding error bars.

A

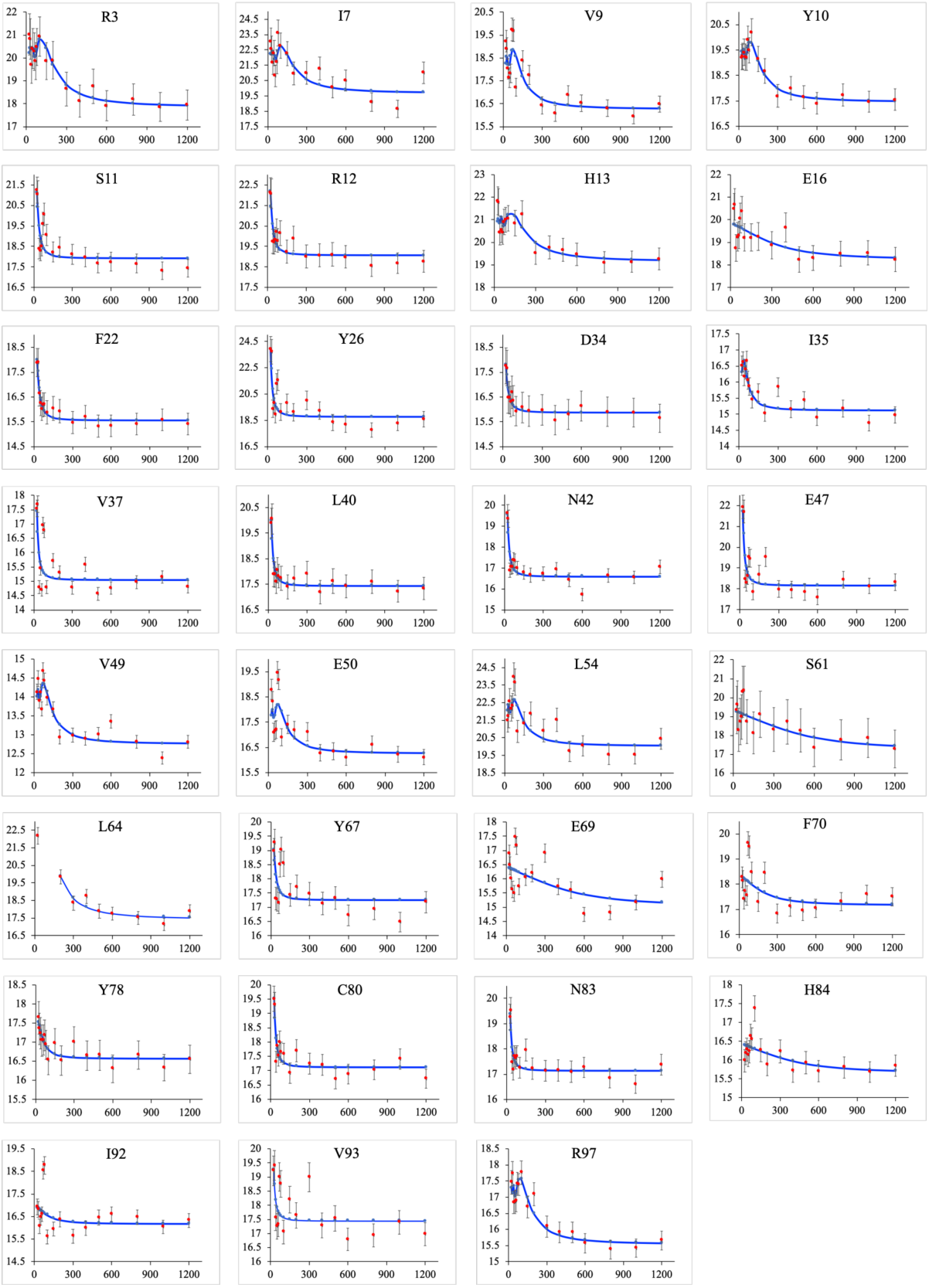

B

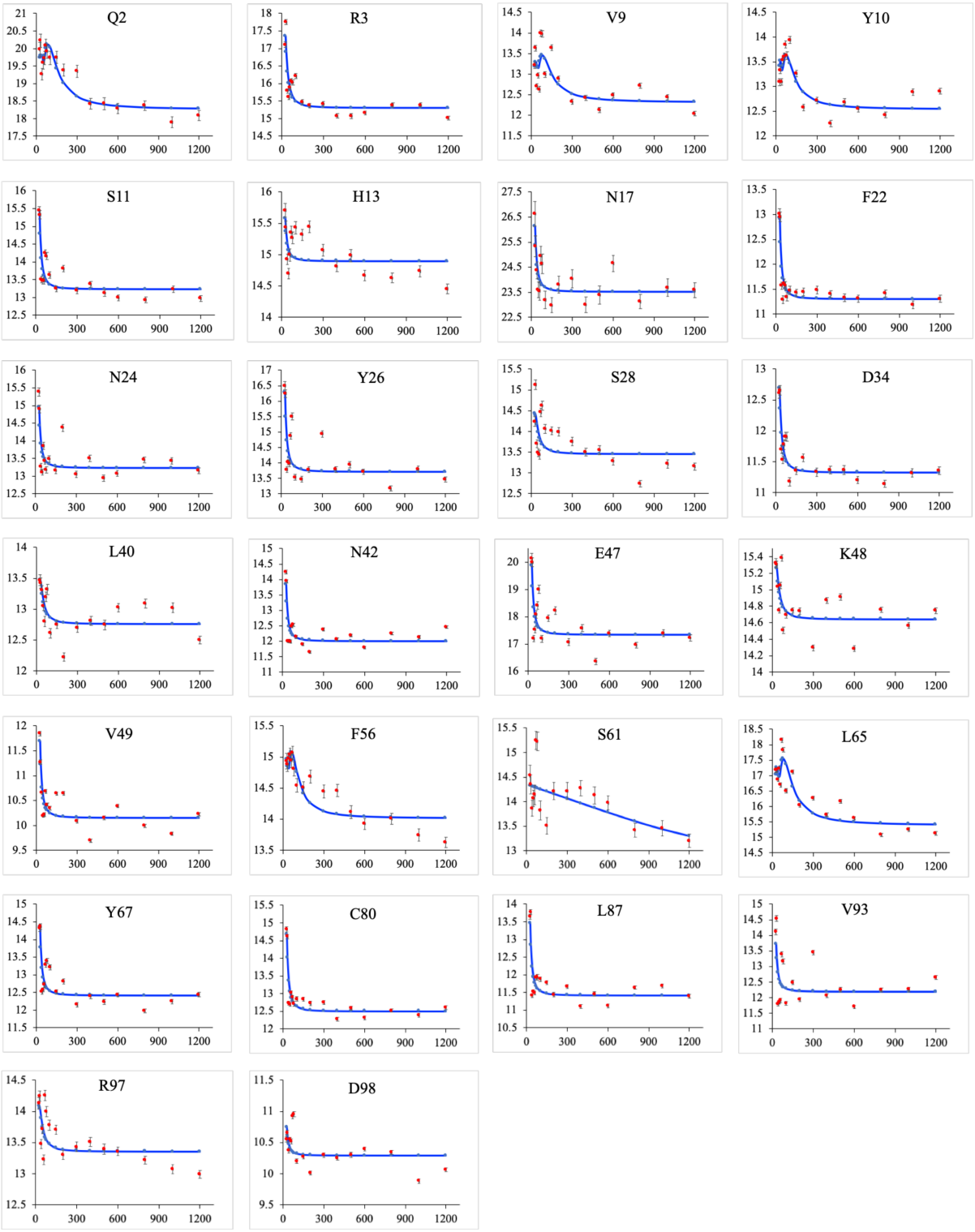
Q2
R3
V9
Y10
S11
H13
N17
F22
N24
Y26
S28
D34
L40
N42
E47
K48
V49
F56
S61
L65
Y67
C80
L87
V93
R97
D98

Table S1: Parameters for the fitting of the curves reported in Figure S7 as obtained from the dedicated routine of Dynamics Center software package (Bruker)[a]. The values of χ^2 (Pearson's χ^2 test statistic) and the related probability density function are reported for each fitted data set.

298K						
Name	R_2^0 [1/s]	Error	k_{ex} [1/s]	Error	χ^2	p-density
R3	17.86	0.79	2.46	1.18	1.13E-01	1.72E-13
I7	19.66	0.77	2.55	0.87	4.44E-01	2.10E-09
V9	16.26	0.28	2.13	0.40	3.80E-01	7.35E-10
Y10	17.46	0.40	1.95	0.54	3.66E-02	6.68E-17
S11	17.93	0.28	117	14	4.29E-01	1.68E-09
R12	19.06	0.32	112	16	1.72E-01	3.12E-12
H13	19.15	0.68	1.81	0.99	1.39E-01	7.42E-13
E16	18.23	0.38	2066	11	2.35E-01	2.76E-11
F22	15.55	0.29	2.4	11.6	4.53E-02	4.08E-16
Y26	18.78	0.36	38.0	5.7	8.79E-01	2.02E-07
D34	15.87	0.35	129	30	4.53E-02	2.99E-16
I35	15.12	0.18	1.27	0.31	9.04E-02	3.67E-14
V37	15.05	0.14	22.0	27.4	5.86E-01	1.36E-08
L40	17.44	0.27	46.8	26.9	9.2 E-02	4.15E-14
N42	16.6	0.19	25.8	22.2	1.67E-01	2.57E-12
E47	18.17	0.23	27.4	25.2	3.97E-01	9.83E-10
V49	12.76	0.14	1.32	0.20	8.53E-02	2.43E-14
E50	16.26	0.27	1.60	0.40	3.84E-01	7.84E-10
L54	20.04	0.54	2.15	0.70	4.49E-01	2.30E-09
S61	17.21	0.71	3032	29	3.09E-01	1.78E-10
L64	17.43	0.42	4.94	1.63	4.28E-02	2.01E-16
Y67	17.24	0.23	119	30	4.20E-01	1.44E-09
E69	15.01	0.17	2907	4	4.10E-01	1.22E-09
F70	17.17	0.25	1237	8	4.21E-01	1.49E-09
Y78	16.56	0.23	324	24	3.36E-02	3.72E-17
C80	17.12	0.21	51.0	27.2	1.23E-01	3.20E-13
N83	17.14	0.23	41.2	29.4	1.40E-01	7.69E-13
H84	15.64	0.20	2512	21	1.12E-01	1.58E-13

I92	16.17	0.21	729	17	6.42E-01	2.53E-08
V93	17.44	0.26	6.4	22.0	4.89E-01	4.06E-09
R97	15.54	0.28	1.68	0.38	8.27E-02	1.97E-14

310K

Name	R_2^0 [1/s]	Error	k_{ex} 1/s]	Error	χ^2	p-density
Q2	18.26	0.12	1.53	0.17	8.40E-02	2.20E-14
R3	15.3	0.08	123	10	1.44E-01	9.18E-13
V9	12.31	0.09	0.94	0.18	1.82E-01	4.69E-12
Y10	12.53	0.11	0.91	0.24	7.78E-02	1.29E-14
S11	13.22	0.05	29.7	25.7	1.79E-01	4.17E-12
H13	14.9	0.05	4.4	31.5	1.02E-01	8.51E-14
N17	23.52	0.20	45.7	25.1	2.29E-01	2.29E-11
F22	11.31	0.04	16.2	30.0	5.80E-02	1.66E-15
N24	13.23	0.05	24.8	17.0	2.12E-01	1.32E-11
Y26	13.72	0.06	21.4	23.0	4.79E-01	3.55E-09
S28	13.45	0.05	0.80	0.33	2.93E-01	1.25E-10
D34	11.33	0.04	1.91	6.68	5.88E-02	1.83E-15
L40	12.75	0.05	0.59	0.25	7.65E-02	1.15E-14
N42	12.01	0.03	14.7	25.7	1.82E-01	4.76E-12
E47	17.33	0.07	17.0	15.0	4.15E-01	1.34E-09
K48	14.64	0.05	0.57	0.38	6.02E-02	2.15E-15
V49	10.15	0.02	23.6	18.6	1.13E-01	1.70E-13
F56	14.02	0.15	0.87	0.39	5.57E-02	1.25E-15
S61	12.57	0.10	7522	1	2.18E-01	1.62E-11
L65	15.4	0.08	1.77	0.13	1.72E-01	3.11E-12
Y67	12.42	0.03	28.6	26.5	2.21E-01	1.79E-11
C80	12.5	0.03	17.8	24.1	9.37E-02	4.70E-14
L87	11.42	0.03	17.6	23.4	2.08E-01	1.18E-11
V93	12.19	0.04	21.4	20.1	6.11E-01	1.81E-08
R97	13.36	0.04	0.60	0.24	1.11E-01	1.49E-13
D98	10.29	0.02	35.9	40.6	1.09E-01	1.38E-13

[a]The routine employed by Dynamics Center models the experimental data with the best fitting out of three different functions, depending on whether the dispersion curve is flat (independent on the effective field), or modulated by slow or fast exchange rate. In the slow exchange limit, the fitting function is[13]:

$$\boldsymbol{R_2(\tau_{CP}) = R_2^0 + k_{ex} - k_{ex}\frac{\sin(\Delta_\omega \tau_{CP})}{\Delta_\omega \tau_{CP}}}$$

where $R_2(\tau_{CP})$ is the transverse relaxation rate determined as a function of time between the CPMG 180° pulses, τ_{CP}, R_2^0 is the transverse relaxation rate without exchange contribution, k_{ex} is the exchange rate constant, Δ_ω is the chemical shift difference between the two exchanging states. The other function used by Dynamics Center to fit relaxation dispersion data refers to the fast exchange limit[14]:

$$\boldsymbol{R_2(\tau_{CP}) = R_2^0 + \frac{\Phi_{ex}}{k_{ex}}\left[1 - \frac{2\tanh\left(\frac{k_{ex}\tau_{CP}}{2}\right)}{k_{ex}\tau_{CP}}\right];\ \Phi_{ex} = p_A p_B \Delta_\omega^2}$$

where p_A and p_B are the fractional populations of the two exchanging states.

Table S2: Selected ^{15}N NMR $T_{1\rho}$ values at different spin-lock field strengths of 0.32 mM β2m measured at 60.82 MHz (^{15}N frequency) and 298 K[a].

Residue	$T_{1\rho}$ [ms] SL=3.00 kHz	$T_{1\rho}$ [ms] SL=1.67 kHz
Q2	94±5	84±3
I7	91±5	83±3
H13	76±2	64±3
F22	91±3	74±3
Y26	86±4	75±6
G29	95±19	82±23
D34	78±10	65±2
E36	96±7	88±5
L40	85±2	76±2
N42	95±7	90±3
K48	87±3	75±3
S55	74±4	53±5
F56	80±3	59±3
D59	68±1	53±5
S61	90±5	85±10
L64	84±5	65±11
E69	95±8	83±4
C80	86±3	73±5
L87	81±2	79±2
V93	94±9	81±3
K94	90±5	85±8
D96	87±6	84±7
R97	96±5	90±5
D98	119±5	94±5

[a] $T_{1\rho}$ measurements were performed with the sequence of Daye and Wagner[16] using spin-lock field strengths (SL) of 3.00 and 1.67 kHz and 20 spin-lock intervals ranging between 0 and 160 ms, with 3 repetitions at short, medium and large intervals for error estimation. The HSQC detection was performed with quadrature in F1 obtained by Echo/Antiecho-TPPI, gradient coherence selection and flip-back pulse for solvent suppression[17-19]. In all measurements, an interscan relaxation delay of 3 s was allowed. The number of scans for each collected relaxation interval was 32. The experiments were acquired in the pseudo3d mode and processed with the Bruker Dynamics Center software. Offset corrections[15] were applied.

References

1 L. Strominger, D. C. Wiley, P. J. Bjorkman, M. A. Saper, B. Samraoui and W. S. Bennett, Structure of the human class I histocompatibility antigen, HLA-A2, *Nature*, 1987, **329**, 506–512.

2 F. Fogolari, A. Corazza, V. Yarra, A. Jalaru, P. Viglino and G. Esposito, Bluues: A program for the analysis of the electrostatic properties of proteins based on generalized Born radii, *BMC Bioinformatics*, 2012, **13**, S18.

3 I. Walsh, G. Minervini, A. Corazza, G. Esposito, S. C. E. Tosatto and F. Fogolari, Bluues server: Electrostatic properties of wild-type and mutated protein structures, *Bioinformatics*, 2012, **28**, 2189–2190.

4 D. Sezer, J. H. Freed and B. Roux, Parametrization, molecular dynamics simulation, and calculation of electron spin resonance spectra of a nitroxide spin label on a polyalanine α-helix, *J. Phys. Chem. B*, 2008, **112**, 5755–5767.

5 J. Gasteiger and M. Marsili, Iterative partial equalization of orbital electronegativity-a rapid access to atomic charges, *Tetrahedron*, 1980, **36**, 3219–3228.

6 R. Skeel, M. Bhandarkar, R. Brunner, A. Gursoy, N. Krawetz, J. Phillips, A. Shinozaki, K. Varadarajan and K. Schulten, NAMD2: Greater Scalability for Parallel Molecular Dynamics, *J. Comput. Phys.*, 1999, **151**, 283–312.

7 D. Bashford and D. A. Case, Generalized born models of Macromolecular solvation effects, *Annu. Rev. Phys. Chem.*, 2000, **51**, 129–152.

8 A. Onufriev, D. Bashford and D. A. Case, Exploring Protein Native States and Large-Scale Conformational Changes with a Modified Generalized Born Model, *Proteins Struct. Funct. Genet.*, 2004, **55**, 383–394.

9 F. Fogolari, A. Corazza, S. Toppo, S. C. E. Tosatto, P. Viglino, F. Ursini and G. Esposito, Studying interactions by molecular dynamics simulations at high concentration, *J. Biomed. Biotechnol.*,2012, **2012**, 1-9.

10 C. J. Dongmo Foumthuim, A. Corazza, G. Esposito and F. Fogolari, Molecular dynamics simulations of β2-microglobulin interaction with hydrophobic surfaces, *Mol. Biosyst.*, 2017, **13**, 2625–2637.

11 T. Grycuk, Deficiency of the Coulomb-field approximation in the generalized Born model: An improved formula for born radii evaluation, *J. Chem. Phys.*, 2003, **119**, 4817–4826.

12 M. F. Sanner, A. J. Olson and J. C. Spehner, Reduced surface: An efficient way to compute molecular surfaces, *Biopolymers*, 1996, **38**, 305–320.

13 M. Tollinger, N. R. Skrynnikov, F.A.A. Mulder, J.D. Forman-Kay and L.E. Kay, Slow Dynamics in Folded and Unfolded States of SH3 Domain, *J. Am. Chem. Soc.*, 2001, **123**, 11341-11352.

14 E.L. Kovrigin, J.G. Kemp, M.J. Grey and J.P. Loria, Faithful estimation of dynamics parameters from CPMG relaxation dispersion measurements, *J. Magn. Reson.*, 2006, **180**, 93-104.

15 A.G. Palmer III and H. Koss, Chemical Exchange, *Methods Enzymol.*, 2019, **615**, 177-236.

16 K.T. Dayie and G. Wagner, Relaxation Rate Measurements for ^{15}N-^{1}H Groups with Pulsed Field Gradients and Preservation of the Coherence Pathways, *J. Magn. Reson.*, 1994, **111**, 121-126.

17 A.G. Palmer, J. Cavanagh, P .E. Wright and M. Rance, Sensitivity improvement in proton-detected two-dimensional heteronuclear correlation NMR spectroscopy, *J. Magn. Reson.*, 1991, **93**, 151-170.

18 J. Schleucher, M. Schwendinger, M. Sattler, P. Schmidt, O. Schedletzky, S.J. Glaser, O.W. Sorensen and C. Griesinger, A general enhancement scheme in heteronuclear multidimensional NMR employing pulsed field gradients, *J. Biomol. NMR*, 1994, **4**, 301-306.

19 S. Grzesiek and A. Bax, The importance of not saturating water in protein NMR. Application to sensitivity enhancement and NOE measurements, *J. Am. Chem. Soc.*, 1993, **115**, 12593–12594.